Radar and LiDAR Sensorfusion in Low Visibility Environments

Paul Fritsche[1], Simon Kueppers[2], Gunnar Briese[2] and Bernardo Wagner[1]
[1]*Institute of Systems Engineering - Real Time Systems Group, Leibniz Universität Hannover, Appelstr. 9A, 30167 Hannover, Germany*
[2]*Fraunhofer Institute for High Frequency Physics and Radar Techniques FHR, Fraunhoferstr. 20, 53343 Wachtberg, Germany*

Keywords: Mobile Robotics, Low Visibility Environments, FMCW-Radar, LiDAR, Sensorfusion, Smoke Detection.

Abstract: LiDAR sensors are unable to detect objects that are inside or behind dense smoke, fog or dust. These aerosols lead to problems for environmental modeling with mobile robotic platforms. For example, if a robot equipped with a LiDAR is surrounded by dense smoke, it can neither localize itself nor can it create a map. Radar sensors, on the other hand, are immune to these conditions, but are unable to represent the structure of an environment in the same quality as a LiDAR due to limited range and angular resolution. In this paper, we introduce the mechanically pivoting radar (MPR), which is a 2D high bandwidth radar scanner. We present first results for robotic mapping and a fusion strategy in order to reduce the negative influence of the aforementioned harsh conditions on LiDAR scans. In addition to the metric representation of an environment with low visibility, we introduce the LRR (LiDAR-Radar-Ratio), which correlates with the amount of aerosols around the robot discussing its meaning and possible application.

1 INTRODUCTION

In many areas of field and rescue robotics, it is essential to have a precise model of an environment. For example, in disaster operations, fire and smoke create situations dangerous for human life. To get a clear picture of the scenario ahead, a mobile platform with sensors that are able to handle harsh conditions, is sent in to record the map necessary for operational planning and orientation. Commonly, standard sensors like LiDAR scanners, sonar sensors and stereo cameras have established themselves as state-of-the-art for most tasks in indoor robotics. Radar sensors appear in field and rescue robotics. They are, however, not used frequently to perform tasks like mapping and localization, due to their limited range and angular resolution.

Commercially available radar sensors have a legally restricted band width, resulting in a limited range resolution of frequency modulated continuous wave (FMCW) radars, thus making them unsuitable for indoor environments. This is one of the reasons why research groups that apply radar in mobile robotics, often use self built sensors. The first appearance of radar sensors in the robotic community is tracing back to the Australian Centre for Field Robotics (ACFR) in the nineties, where fundamental work on probabilistic SLAM algorithms in combination with radar was developed (Clark and Dissanayake, 1999). Also, they built their own radar scanner (Clark and Whyte, 1998). Besides the ACFR, Adams et al. (Adams and Jose, 2012) were doing research on radar in robotics with the integration of the PHD filter and the application for mapping of mines. The PHD SLAM is working with a commercial NavTech device. In contrast to the feature based SLAM approaches, Vivet et al. (Vivet et al., 2013) use scan matching through a Fourier-Mellin transform with the custom made K2PiMMW scanner producing large scale maps. Mapping of indoor environments was performed by Detlefsen (Detlefsen et al., 1993) and Marck (Marck et al., 2013). We have been studying the use of low bandwidth FMCW sensors for robotic mapping using a rotating scanner setup with lateration and lope offsets (Fritsche and Wagner, 2015). Together with an international team, Sakamoto presented the application of a modified version of his inverse boundary scatter transform (IBST) and Kirchhoff migration, a SAR algorithm, for an environmental imaging with a mobile robot (Salman et al., 2013). Most SAR algorithms are very sensitive toward noise, which makes it difficult to apply them in robotic mapping. A sensor fusion between radar and LiDAR for obstacle avoidance was realized by Yamauchi (Ya-

Fritsche, P., Kueppers, S., Briese, G. and Wagner, B.
Radar and LiDAR Sensorfusion in Low Visibility Environments.
DOI: 10.5220/0005960200300036
In *Proceedings of the 13th International Conference on Informatics in Control, Automation and Robotics (ICINCO 2016) - Volume 2*, pages 30-36
ISBN: 978-989-758-198-4

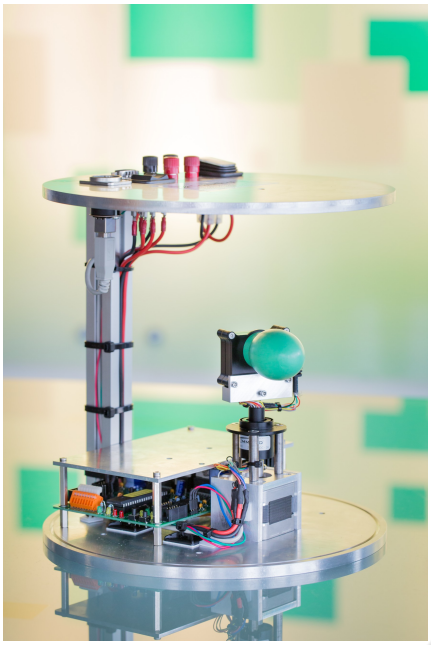

Figure 1: Picture of Mechanically Pivoting Radar.

mauchi, 2010).

Section 2.1 describes the functionality of the mechanically pivoting radar (MPR). The comparison of MPR and two other sensor for the same purpose is given in Section 2.2. Section 2.3 presents our scan fusion method and the LiDAR-Radar-Ratio (LRR). Experiments described in Section 3 provide the implementation of our methods. Section 4 brings out the results and discusses limitations and possible applications. Finally, Section 5 sums up our results describing our contribution.

2 METHODS

The following section explains principles behind the MPR comparing it with a Velodyne VLP-16 as well as with a NavTech MMW radar scanner. Then, we focus on the integration of radar and LiDAR measurements, in order to reduce the influence of aerosols on LiDAR scans. The fused scan suits for modeling of low visibility environments. Furthermore, we introduce the LRR, which correlates with the amount of smoke inside an environment.

2.1 The MPR - A 2D FMCW Radar Scanner

The development of the MPR system has been carried out by the Fraunhofer Institute for High Frequency Physics and Radar Techniques in order to provide hardware for a radar based approach for two-dimensional scanning. Its principle function is comparable to a regular laser scanning unit, where a mechanically rotating element is used to generate a continuously revolving beam. As it can be seen in Figure 1 the MPR hardware consists of a compact USB controlled FMCW radar unit, that is based on a custom MMIC with 80 GHz center frequency and a maximum sweep bandwidth of 25 GHz providing a range resolution of about 6 mm $(self-citation)$. A slip ring has been used up to the USB data and power lines in order to allow the FMCW radar beam to be rotated continuously in the azimuth plane. The rotary movement was realized using stepper motors controlled via a commercially available stepper motor controller. The overall mechanical dimensions are 250 millimeters in diameter and 275 millimeters in height.

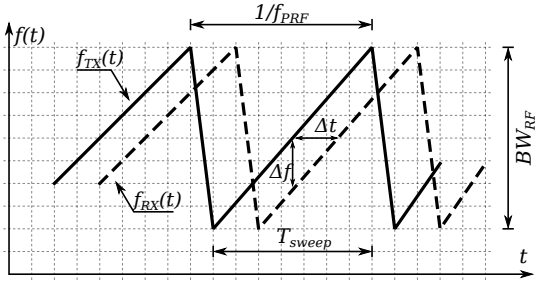

Figure 2: Frequency-over-time plots of transmit and receive signal in linear frequency modulated continuous wave radars.

In order to present the operation of the USB radar unit, Figure 2 shows the basic relationship between the momentary frequency of the transmitted signal $f_{TX}(t)$ and the received signal $f_{RX}(t)$ in an FMCW based radar system with a single stationary target reflection. As can be seen, the transmitted signal (solid line) is a linear frequency sweep covering a frequency bandwidth of BW_{RF} over T_{sweep}. This signal is radiated using an appropriate antenna structure. Due to the propagation delay of the emanated electromagnetic waves, the reflected signal (dashed line) of the target is delayed by a time delay of Δt once received by the radar system. From this observation, the basic relationship of target distance R to time delay Δt can be described as shown in Equation 1.

$$R = \frac{c}{2}\Delta t \tag{1}$$

Due to the linear frequency modulation, the frequency offset Δf indicated in Figure 2 has a direct relationship to the time delay Δt introduced by the propagation delay as described previously. It is proportional with a factor of BW_{RF}/T_{sweep}. Thus the distance R to

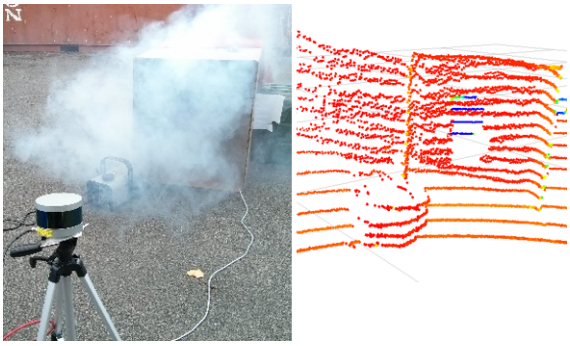

Figure 3: Left: Stationary LiDAR scanner in front of a box, which is filled with fog. Right: 3D scan image of the Velodyne VLP-16 showing the detection of fog.

a single target can be evaluated from the frequency difference Δf as shown in Equation 2.

$$R = \frac{c \cdot T_{sweep}}{2 \cdot BW_{RF}} \Delta f \tag{2}$$

Through the use of frequency mixing, the frequency offset Δf can be extracted with little effort. The resulting intermediate frequency (IF) signal is a linear superposition of the above described relationships for all targets visible by the radar system. Further processing of the radar information is then done by digitizing the IF signal and using algorithms such as Fast-Fourier-Transform and peak detection in the digital domain to extract range information for multiple targets.

With a rotary resolution of 1.8 degrees, a maximum of 200 radar acquisitions can be resolved during one rotation of the radar unit. At the maximum rotation rate of 2.5 Hz, up to 500 single radar acquisitions are carried out per second, while the radar is continuously scanning in the azimuth plane. The measurement range of the MPR is between 0.2 meters to about 15 meters, depending on the type of target to be detected.

2.2 Comparing the MPR

As mentioned before, aerosols influence the measurement quality of LiDAR significantly. The reason for the radar not being affected by aerosols is that the wave length of radar is larger than most aerosol particles. For example, dust is larger than 0.5 μm and smoke particles are submicrometer in size (Willeke et al., 1993, p. 5). Dense fog, as can be seen in Figure 3, gets detected by the Velodyne VLP-16, even if the strongest return echo is selected. On the other hand, radar scanners cannot represent an environment in the same quality as LiDAR scanners. Table 1 summarizes the most important sensor properties of the

Table 1: Comparing Velodyne VLP-16, MPR and NavTech MMR radar.

	Velodyne VLP-16	MPR	NavTech MMW radar
Measurement range	up to 100 m	up to 15 m	up to 200-800 m
Angular resolution	0.1-0.4°	1.8°	0.09°
Beam width	0.17°	4.9°	1.8°
Wave length	903 nm	3.26-3.41 mm (88-92 GHz)	3.89-3.95 mm (76-77 GHz)
Scan rate	5-20 Hz	2.5 Hz	2.5 Hz

Velodyne VLP-16, the MPR and the NavTech MMW Radar, which was used by Adams (Adams and Jose, 2012, p. 329).

The measurement range depends mainly on the power of the emitted radar wave, the focussing of the antenna, the radar cross section (RCS) of the object and the detection algorithm. NavTech radars are meant for airport and vehicle traffic surveillance and work accordingly with a stronger emitting power. The angular resolution refers to the steps between two measurements. The NavTech Radar has the highest angular resolution, but its wide beam width results in a blurry scan image. Due to large beam widths, radar scanners usually measure the same object from more than one angular step, which leads to a sickle-shaped representation of objects inside a radar scan. The MPR has a sweep bandwidth of 4 GHz, which corresponds according to Equation 3 to a distance resolution of 3.75 cm.

$$\Delta R = \frac{c}{2 \cdot BW_{RF}} \tag{3}$$

A radar's resolution is its capability to distinguish objects. Usually, the distance accuracy is higher. One MPR scan contains 200 single radar acquisitions. Due to radar's technical principle, radar scanners have slower scan rates compared to 2D LiDAR scanners, which even exist with 100 Hz.

2.3 Integrating MPR- and LiDAR-Scans

The fusion of LiDAR and radar scans to a fused scan combines the advantages of both sensors. Usually, a scan message contains an array of range measurements $S = [R_0, R_1, ..., R_n]$. We diminish outliers inside radar scans, which are caused by reflections and

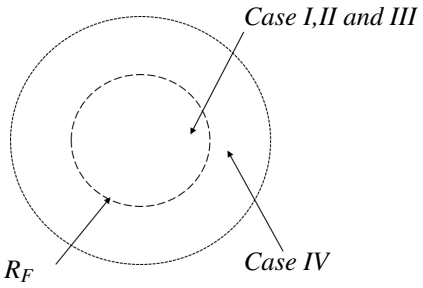

Figure 4: This drawing depicts the overlapping scan fields.

wrong detection, by applying a local outlier factor (LOF) filter (Breunig et al., 2000). Our proposed fusion method replaces a LiDAR point $R_{i,LiDAR}$ of a 2D scan, which is affected by smoke, with a corresponding radar points $R_{j,Radar}$, according to the sensor setup in Figure 5.

In general, different sensors have different scan ranges. In our case, the LiDAR has a larger scan range than the radar. This basically depends on the emitted power, the focusing of the antenna and the sensitivity of the detection algorithm. The maximum range of LiDAR and radar is not constant also depending on the reflectivity of the objects inside the scene. Therefore, a sensor fusion can only be performed in overlapping scan fields, which can be determined dynamically through the fusion range R_F depending on the average range of a radar scan $R_{Radar,\varnothing}$, the maximum range of a radar scan and the parameter $\alpha = [0..1]$.

$$R_F = R_{Radar,\varnothing} + \alpha(R_{Radar,max} - R_{Radar,\varnothing}) \quad (4)$$

Inside the fusion range, there can be three cases to form a fused scan, as shown in Figure 4.

- Case I: $||R_{LiDAR} - R_{Radar}|| < \beta : R_{Fusion} = R_{LiDAR}$
  If the corresponding pair of points from LiDAR and radar do not have a larger Euclidean distance to each other than a pre-defined parameter β, then the LiDAR point is used to build the fused scan.
- Case II: $R_{LiDAR} < R_{Radar} : R_{Fusion} = R_{Radar}$
  If there are aerosols in the air, the corresponding LiDAR points are in front of the radar points.
- Case III: $R_{LiDAR} > R_{Radar} : R_{Fusion} = R_{Radar}$
  Some rare objects, which have, for example, elements of a metal grid or mesh, reflect radar, but let LiDAR shine through it.

Outside the overlapping scan fields, only LiDAR points contribute to the fused scan.

- Case IV: $R_{LiDAR} > R_F : R_{Fusion} = R_{LiDAR}$
  The maximum measurement range of our radar is lower. The fused scan will keep LiDAR points, which are larger than the average radar distance.

Figure 5: This figure shows the setup of the experiment. It has been performed in a yard with a robotic platform, which is equipped with the 2D MPR and a 3D Velodyne VLP-16 LiDAR.

The experiments of this paper were performed with $\alpha = 0$.

Every point of the fused 2D scan contains the information, from which case, it has been derived. In this article, we propose the calculation of the LRR.

$$LRR = \frac{\sum R_{Fusion} \in CaseII}{\sum R_{Fusion}} \quad (5)$$

The LRR can represent the amount of smoke in an environment, but is not related to the density. On the other side, objects which cannot be detected by the radar lead to an increasing of the LRR as well. In this article, we will monitor the LRR during the presence of fog and during the presence of objects, which are invisible for radar. Since smoke sensors are usually very slow, the LRR can be used for faster smoke detection.

3 EXPERIMENTS

Before performing our main experiment, we wanted to see if it is possible to integrate MPR scans into scan registration based SLAM approaches, because previous studies indicate that due to most radar scanner's bad accuracy and resolution, the focus has been on feature based SLAM approaches. Therefore, we drove up and down a corridor of our building with a Pioneer platform and recorded radar and LiDAR data.

The main experiment was performed inside a yard where we were able to generate fog with a fog machine to simulate low visibility conditions. This experiment was carried out to find out about the affect

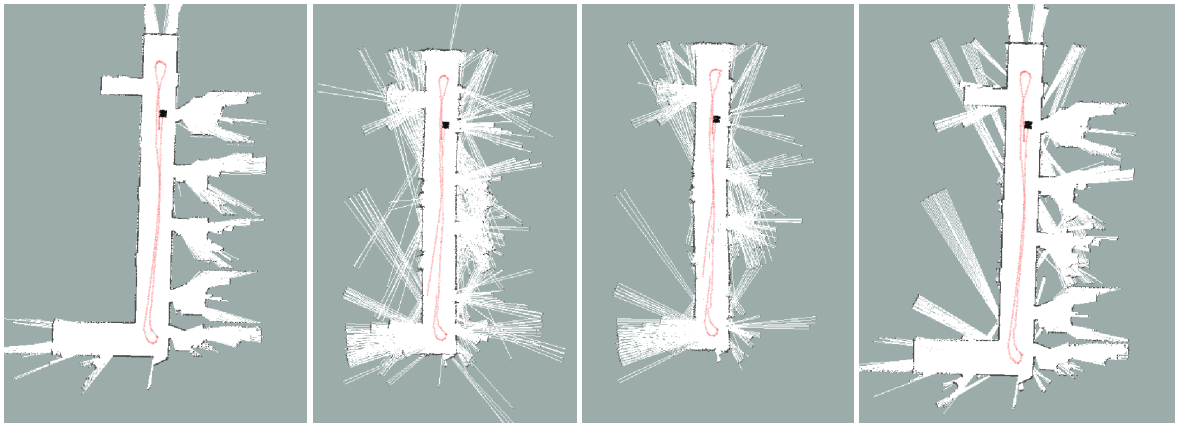

(a) Velodyne VLP-16 (b) MPR (c) MPR and LOF filtering (d) Velodyne and MPR fusion

Figure 6: These maps reveal first results including the MPR for robotic mapping.

of aerosols on robotic mapping, observing our fusion method and the LRR. As can be seen from Figure 5, we equipped a Pioneer platform with a Velodyne VLP-16 and the MPR.

Our software was implemented via the middleware ROS. In order to remotely control the Pioneer, we used the rosaria driver package. Furthermore, we applied the Velodyne stack to get sensor reading from the LiDAR and the standard ROS SLAM tool *gmapping* (Grisetti, 2005).

4 RESULTS AND DISCUSSION

FHR have introduced a new radar scanner, for mapping and localization in low visibility environments. Figure 6 presents grid maps of a corridor and the estimated robot trajectories. Figure 6(a) and Figure 6(b) visualize the difference between maps that have been built with LiDAR and radar. Obviously, the LiDAR scanner results in a clearer map than the MPR and the robot's trajectory jumps while using the MPR for SLAM. But, to the author's knowledge, not many successful implementation of radar for grid based mapping with simultaneous localization in an indoor environment were achieved. We believe, this is due to the very good sensor specification of the MPR (and due to the robustness of *gmapping*). However, there are Marck et al. (Marck et al., 2013) who applied ICP between two consecutive radar scans. Other publications address mapping ((Brooker et al., 2005), (Adams and Jose, 2012, p. 18), (Fritsche and Wagner, 2015)) but with known sensor locations or feature based SLAM (Clark and Dissanayake, 1999).

As shown in Figure 6(c), outliers inside the resulting map can be diminished via LOF filtering, although it is not possible to erase them completely. Consequently, if an environment does not contain any smoke, fog or dust, then a radar scanner has no advantageous over a LiDAR scanner. Our fusion method enhances the resulting map under normal conditions. Since we are not able to suppress all outliers, the map (Figure 6(d)) still contains more spikes than the pure LiDAR map.

The advantage of our fusion method is depicted in Figure 7. Figure 7(a) and 7(b) reveal one scan image of the MPR and the Velodyne VLP-16 (horizontal cut) with the presence of fog, which is marked via a yellow circle. As can be seen from Figure 7(c), the scan fusion replace LiDAR points which are affected by fog with radar points, in order to get a clean scan for localization, mapping or SLAM. This permits making structure visible, which is inside or behind aerosols. At the same time, our fusion method gives LiDAR the priority when aerosols are absent. The used fog machine could not generate enough fog to keep the environment very nebulous for a long time, because it needs to recharge frequently. During a real rescue scenario, which involves fire and smoke, there can be more occlusion.

But, there is one situation, we should have a closer look at: If an object can be detected by the LiDAR, but cannot be detected by the radar and it is inside the fusion range R_F, then it gets erased from the scan, because the conditions regarding the cases are the same as in case II. If the radar detects nothing, the LiDAR should not be used consequently, because there can be smoke for example in front of an open scene.

As a further aspect of the LiDAR and radar scan integration, we introduced the LRR. Common gas sensors and smoke detectors are disadvantageous as they have a slow respond time and measure only one certain point. Additionally, the measurement proce-

(a) MPR scan.

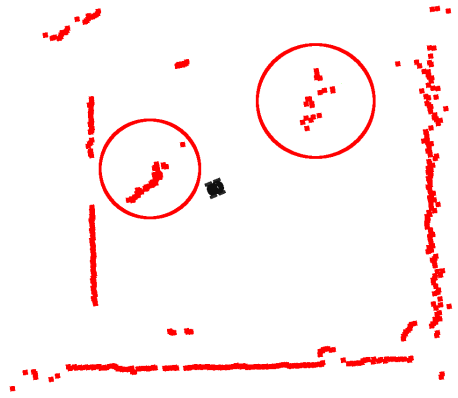

(b) Velodyne VLP-16 scan.

(c) Fused scan.

Figure 7: 7(a): Scan with the MPR. 7(b): 2D scan (horizontal cut of 3D scan) of the Velodyne VLP-16. The red circle marks an area, where LiDAR detects fog. 7(c): Our sensorfusion replaces LiDAR point, which are affected by fog, with radar points. Red points represent case I, green points represent case II and magenta points represent case IV.

dure requires a stationary setup, so if a gas sensor is placed on a mobile robot, the result is not clearly interpretable. Usually, gas and smoke distributions are highly dynamic and the movement of the robot itself creates a swirling. Consequently, it is very hard to model fog or smoke in an environment. The LRR can give a remarkably quick information about the amount of aerosols and objects which cannot be detected by radar inside the fusion range.

During the experiments that we performed in the yard, we let the robot stay for 40 seconds and started driving afterwards. After approximately 50 seconds, we turned on the fog machine for 10 seconds. This phase is marked yellow in Figure 8.

The LRR correlates accordingly to the amount of fog in the yard. On one side of the yard, there is a big hedge and at 75 second we drove the robot close to the hedge, so that it was inside the fusion range R_F. We observed that the hedge cannot be detected with the MPR. Consequently, case II of our algorithm handles

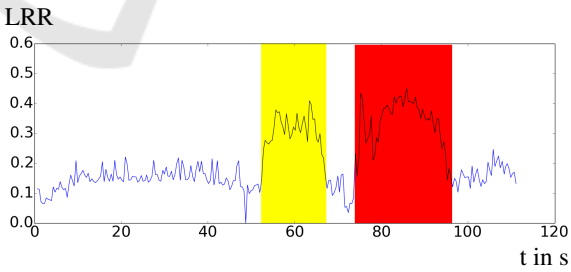

Figure 8: The LRR raises if the robot is surrounded by fog (yellow). If, the robot drives close to an object (closer than $R_{\varnothing,radar}$), which cannot be detected by the radar, then the LRR raises as well (red).

it if it were fog. Future work will include a geometry detection, for example lines, in order to distinguish smoke from structured shapes, which are invisible for the radar. Afterwards, we drove away from the hedge. This phase is marked red on the diagram in Figure 8 and cannot be distinguished from the yellow phase.

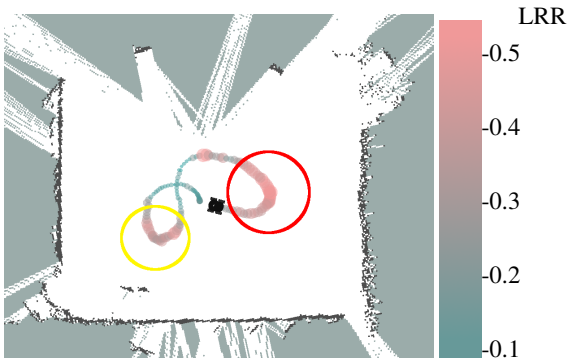

Figure 9: This figure presents the LRR visualization during robotic navigation.

Figure 9 shows a grid map, which was generated with the fused scan and the ROS SLAM tool *gmapping*. The outliers are caused by the MPR, but can be reduced by filtering the MPR scan, for example via radial outlier removal, before fusing it with the LiDAR. The LRR is visualized along the robot path in the grid map as well.

Equivalent to Figure 8, the yellow circle presents the phase with operating fog machine and the red circle marks the phase, where the robot is too close to the hedge. A map or trajectory containing LRR information can give the operator additional information about an environment. The LRR can be used as an alert signal for operators to make them control the robot more carefully. It could be used to trigger the measurement of gas sensors.

5 CONCLUSION

With this work we have shown that the MPR is a useful scanning device and can be used in low visibility environments. The MPR is suitable for applications such as rescue robotics and field robotics. We have developed a new fusion strategy in order to reduce the influence of fog, smoke, dust, etc. on a single LiDAR scan. Our approach enhances the use for scan registration based SLAM, where a clean scan is preferred. Additionally, we introduced the LRR, which can be used as a fast fog or smoke detector under certain conditions. More data sets involving fog or smoke will be needed, for further evaluation of our proposed methods. Future work will include gas and smoke sensors to investigate correlation with the LRR, the integration of a data fusion through joint probability distributions for case I and the investigation of outlier reduction methods for radar data.

ACKNOWLEDGMENT

This work has partly been supported within H2020-ICT by the European Commission under grant agreement number 645101 (SmokeBot).

REFERENCES

Adams, M. and Jose, E. (2012). *Robotic navigation and mapping with radar*. Artech House.

Breunig, M. M., Kriegel, H.-P., Ng, R. T., and Sander, J. (2000). Lof: Identifying density-based local outliers. *ACM SIGMOD International Conference on Management of Data*, 29(2):93–104.

Brooker, G., Scheding, S., Bishop, M., and Hennessy, R. (2005). Development and application of millimeter wave radar sensors for underground mining. *IEEE Sensors Journal*, 5(6):12701280.

Clark, S. and Dissanayake, G. (1999). Simultaneous localisation and map building using milimetre wave radar to extract natural features. *Internation Conference on Robotics and Automation*.

Clark, S. and Whyte, H. D. (1998). The design of a high performance mmw radar system for autonomous land vehicle navigation. In *Field and Service Robotics*.

Detlefsen, J., Rozmann, M., and Lange, M. (1993). 94 hgz 3-d imaging radar sensor for industrial environments. *EARSeL ADVANCEA IN REMOTE SENSING*.

Fritsche, P. and Wagner, B. (2015). Comparison of two radar-based scanning-techniques for the use in robotic mapping. In *Informatics in Control, Automation and Robotics (ICINCO), 2015 12th International Conference on*, volume 01, pages 365–372.

Grisetti, G. (2005). Improving grid-based slam with rao-blackwellized particle filters by adaptive proposals and selective resampling.

Marck, J. W., Mohamoud, A., van Heijster, R., et al. (2013). Indoor radar slam a radar application for vision and gps denied environments. In *Radar Conference (EuRAD), 2013 European*, pages 471–474. IEEE.

Salman, R., Willms, I., Sakamoto, T., Sato, T., and Yarovoy, A. (2013). Environmental imaging with a mobile uwb security robot for indoor localisation and positioning applications. In *Microwave Conference (EuMC), 2013 European*, pages 1643–1646.

Vivet, D., Checchin, P., and Chapuis, R. (2013). Localization and mapping using only a rotating fmcw radar sensor. *Sensors*.

Willeke, K., Baron, P., and Martonen, T. (1993). *Aerosol Measurement: Principles, Techniques and Applications*, volume 6. [New York, NY]: Mary Ann Liebert, Inc., c1988-2007.

Yamauchi, B. (2010). Fusing ultra-wideband radar and lidar for small ugv navigation in all-weather conditions. *Proc. SPIE 7692, Unmanned Systems Technology XII*.